

Article

Impact of Limestone Surface Impurities on Quicklime Product Quality

Matias Eriksson ^{1,2,3,*} , Karin Sandström ^{1,2,4} , Markus Carlborg ^{1,2}  and Markus Broström ^{1,2} 

¹ Centre for Sustainable Cement and Quicklime Production, Department of Applied Physics and Electronics, Umeå University, SE-90187 Umeå, Sweden; karin.sandstrom@umu.se (K.S.); markus.carlborg@umu.se (M.C.); markus.brostrom@umu.se (M.B.)

² Thermochemical Energy Conversion Laboratory, Department of Applied Physics and Electronics, Umeå University, SE-90187 Umeå, Sweden

³ The Swedish Mineral Processing Research Association—MinFo, Marieviksgatan 25, SE-10044 Stockholm, Sweden

⁴ Industrial Doctoral School for Research and Innovation, Umeå University, SE-90187 Umeå, Sweden

* Correspondence: matias.eriksson@umu.se

Abstract: Quicklime is produced through the thermal processing of limestone in industrial kilns. During quarry operations, fine particulate quarry dust adheres to limestone lump surfaces, increasing the bulk concentration of impurities in limestone products. During thermal processing in a kiln, impurities such as Si, Mg, Al, Fe, and Mn react with Ca, reducing quicklime product quality. Which reactant phases are formed, and the extent to which these result in a reduction in quality, has not been extensively investigated. The present study investigated as-received and manually washed limestone product samples from two operational quarries using elemental compositions and a developed predictive multi-component chemical equilibrium model to obtain global phase diagrams for 1000–1500 °C, corresponding to the high-temperature zone of a lime kiln, identifying phases expected to be formed in quicklime during thermal processing. The results suggest that impurities found on the surface of the lime kiln limestone feed reduce the main quality parameter of the quicklime products, i.e., calcium oxide, CaO (s), content by 0.8–1.5 wt.% for the investigated materials. The results also show that, in addition to the effect of impurities, the quantity of CaO (s) varies greatly with temperature. More impurities result in more variation and a greater need for accurate temperature control of the kiln, where keeping the temperature below approximately 1300 °C, that of Hatrurite formation, is necessary for a product with higher CaO (s).

Keywords: calcium oxide; chemical equilibrium calculations; thermal process chemistry



Citation: Eriksson, M.; Sandström, K.; Carlborg, M.; Broström, M. Impact of Limestone Surface Impurities on Quicklime Product Quality. *Minerals* **2024**, *14*, 244. <https://doi.org/10.3390/min14030244>

Academic Editors: Manuel Pozo Rodríguez, Francisco Franco and Michael G. Stamatakis

Received: 21 December 2023

Revised: 23 February 2024

Accepted: 26 February 2024

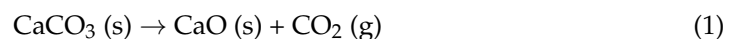
Published: 27 February 2024



Copyright: © 2024 by the authors. Licensee MDPI, Basel, Switzerland. This article is an open access article distributed under the terms and conditions of the Creative Commons Attribution (CC BY) license (<https://creativecommons.org/licenses/by/4.0/>).

1. Introduction

The raw material for quicklime is limestone, an abundant rock that is quarried or mined. Limestone is rich in calcium carbonate CaCO₃ (s), typically occurring as the mineral calcite; this is heated in industrial kilns to temperatures above the carbonate decomposition temperature to produce quicklime, which is rich in calcium oxide CaO (s), according to Reaction 1 as follows:

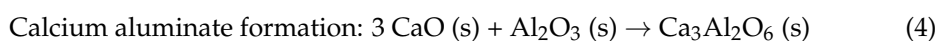
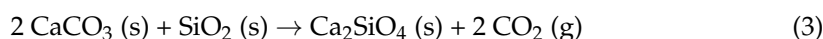
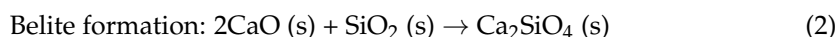


The thermal decomposition, or calcination, of calcite has been extensively studied. Rate-limiting processes have been defined [1], and the effects of steam [2], pressure [3], CO₂ partial pressure [4], heating rate [5], and impurities [6–8], among other parameters, have been identified. Of the proposed calcination mechanisms, a mechanism involving intermediate “activated lime” CaO*(s), originally proposed by Hyatt et al. in 1958 [9], has received support in more recent studies [4,10]. In addition to the calcination process, the thermal behavior of limestone at temperatures below calcination has been studied extensively; see, e.g., [11]. The thermal behavior and properties of different quicklimes and of the main component, calcium oxide CaO (s), produced at low temperatures, 650–1000 °C, has also been studied [12–14].

To reduce the residence time and increase production capacity, the quicklime temperature in a lime kiln reaches 1100–1450 °C [15,16], far exceeding the calcination temperature of 800–900 °C. After calcination, the quicklime continues to exhibit phase transformations as the temperature in the lime kiln increases, and the final phase composition will depend on the maximum temperature reached. Eventually, the final product quality is also influenced by cooling, post-processing such as crushing and sieving, storage, and transport to the end user. The present paper targets the effect of impurities on the quicklime quality, expressed as the calcium oxide CaO (s) content, between 1000 and 1500 °C, corresponding to the high-temperature zone of the lime kiln.

The thermal behavior of quicklime in lime kiln conditions and the suitability of limestone for quicklime production has been extensively investigated, e.g., regarding general suitability [17], block formation tendencies in shaft kilns [18], product reactivity [19–21], thermal decrepitation [22], fuel ash interactions on quicklime surfaces [23,24], interactions of chlorine and sulfur with the quicklime product [25], specific heat capacity [26], and thermal conductivity [27].

Few studies have been found on the phase chemistry of quicklime in the high-temperature zone of a lime kiln. Vola et al. considered phase evolution during quicklime production in generic terms [28] and studied the phase composition of different quicklimes produced at 1050 °C, 1150 °C [29], and 1200 °C [30] in laboratory conditions. Hökfors et al. and Eriksson et al. [31–33] investigated the phase composition of quicklime from high-purity limestone of 97.41 wt.% CaCO₃ (s) in different kiln conditions by utilizing equilibrium calculations at temperatures ranging from 839 to 1774 °C. Previous studies have identified several calcium compounds in quicklime such as CaO (s), CaCO₃ (s), Ca₂SiO₄ (s), Ca₃SiO₅ (s), Ca₃Al₂O₆ (s), Ca₄Al₂Fe₂O₁₀ (s), Ca₃MgSi₂O₈ (s), Ca₂MnO₄ (s), and CaSO₄ (s). Earlier studies have focused on the bulk composition of limestone and singular temperatures or cooled laboratory samples. No studies on the influence of impurities adhered to limestone surfaces on quicklime product quality have been found, nor have studies on the evolution of phases in quicklime in the high-temperature zone of a lime kiln been found. Although the chemistry is complex and not fully known, the main interactions of Ca with impurities can be simplified by reactions (2)–(6) [34–37] as follows:



Quicklime is used in many industrial applications, such as steel production and other metallurgical processes, pulp and paper production, and construction and environmental applications [38,39]. Quicklime is available in a wide range of product qualities [40–42]. The main quality parameter and the main price driver is the CaO (s) content. The world production of quicklime is estimated to be 430 Mt per year [43]. Although kiln setup and fuel properties influence quicklime quality, the quality is primarily dependent on the properties of the limestone feed [33,44].

Limestone can be classified based on the chemical purity of the rock (see Table 1); limestone of higher purity results in quicklime of higher CaO (s) than quicklime produced from lower-purity limestone under similar production conditions. For high-calcium limestone, all compounds other than CaCO₃ (s) are considered impurities. Impurities that originate in materials deposited simultaneously with CaCO₃ (s) and that are dispersed throughout the formation are classified as homogeneous impurities. Impurities that appear as inclusions or as loosely embedded materials formed during the sedimentation process often occur as layers in the deposit [45] and are classified as heterogeneous impurities. Common impurities are clay and siliceous matter, and the major impurity elements are Si,

Al, Fe, and Mg [44,46]. The content of minor elements in commercial limestone is usually low (see Table 2).

Table 1. Classification of high-calcium limestone based on chemical composition, expressed as major oxides, in wt.% [47–49].

Classification	CaO	MgO	SiO ₂	Fe ₂ O ₃
<i>Very high purity</i>	>55.2	<0.8	<0.2	<0.05
<i>High purity</i>	54.3–55.2	0.8–1.0	0.2–0.6	0.05–0.1
<i>Medium purity</i>	52.4–54.3	1.0–3.0	0.6–1.0	0.1–1.0
<i>Low purity</i>	47.6–52.4	>3.0	<2.0	>1.0
<i>Impure</i>	<47.6	>3.0	>2.0	>1.0

Table 2. Typical minor elements in limestone, expressed as oxides, in wt.% [50].

Al ₂ O ₃	BaO	Cr ₂ O ₃	CuO	K ₂ O	Mn ₃ O ₄	Na ₂ O	NiO	P ₂ O ₅	PbO	SO ₃	SrO	TiO ₂	ZnO	ZrO ₂
<0.3	<0.1	<0.1	<0.1	<0.1	<0.1	<0.1	<0.1	<0.1	<0.1	<0.5	<0.2	<0.1	<0.1	<0.1

In quicklime production, elements such as Si, Al, Fe, and Mg can also originate from other sources, e.g., fuel ash. Ash-forming elements in fuels have been related to disturbances in kiln operations and reduced CaO (s) content in the product [15,32,33,51]. Fuel ashes were not considered in this investigation.

The limestone production process comprises operations such as blasting, hauling, crushing, sieving, washing, and sampling, generating small particulate matter, i.e., quarry dust. The amount of quarry dust generated will depend on several parameters, such as the amount of heterogeneous impurities contained in the deposit, e.g., clay layers; whether blasting, crushing, and hauling is performed in a manner that reduces the amounts of small particulates generated; and whether the limestone processing plant is equipped with encapsulation and suction with filters to capture the dust in a controlled way. Although the quarry dust is enriched with soft materials such as clay, the composition generally corresponds to that of the bulk of the quarry. For a limestone quarry, this means significant quantities of Ca. This fine particulate material can adhere to the surface of limestone pebbles fed to the kiln to such an extent that it affects quicklime production and product quality. The amount of adhered quarry dust on the limestone surfaces will depend, not only on the amount of quarry dust available, but also on wind and other weather conditions. The experience of the lime kiln operator is that, especially in cold and wet weather conditions, the amount of adhered quarry dust can be significant, resulting in a clear response in lime kilns. Typical kiln responses are, e.g., reduced quicklime quality; an increase in buildups in the channel system of the kiln, resulting in a decrease in kiln availability; and increased dust load on kiln filters, forcing a reduction in kiln production. The aim of the present study was to generate new knowledge on the impact of impurities that are attached to limestone pebbles on the product quality of quicklime, defined here as calcium oxide and designated CaO (s).

2. Materials and Methods

Limestone samples—A and B—originating from two different northern European quarries were used in this study. Limestone A belongs to the Boda group in central Sweden. The limestone is of Upper Ordovician age, shaped by a meteor during the subsequent Devonian period just over 380 million years ago, and consists of Upper Katian deeper-water carbonate mud-mounds bodies. These bodies overlay lower-to-middle Hirnantian-bedded limestone strata. The limestone is fine- to medium-grained and has a micritic structure. Limestone B belongs to the Slite group on Gotland, Sweden. The Silurian surface bedrock on Gotland spans approximately 10 million years (428–418 million years ago). The bedrock around the deposit consists of a sequence of up to 40 m thick limestone and reef limestone.

Beneath the limestone layers, there are deposits dominated by marl and marlstone with flank deposits.

In Swedish limestone quarries and lime kilns, the influence of wet and cold winter conditions is clearly noticeable and manifests as an increased amount of adhered quarry dust on the limestone products, even if the limestone is recently blasted, such as in this study. Two samples of approximately 15 kg each of lime kiln feed limestone pebbles of the fraction 40–90 mm were collected during the winter period. The samples represent the momentary conditions in the quarry. A washing protocol was undertaken, wherein material on the surface of the limestone products was manually removed by brushing in water, after which, the washed lumps of limestone were removed from the washing water and dried at 105 °C. The washing residue was separated through sedimentation, decanting, and drying at 105 °C.

The elemental compositions of the samples were determined for both as-received and washed conditions. A Panalytical Axios mAX WDXRF X-ray fluorescence (XRF) spectrometer and a Leco CS744 IR carbon and sulfur analyzer (IR-C/S) (LECO Corporation, St. Joseph, MI, USA) were used to determine the elemental compositions. Chlorine content was not analyzed in the present study but was estimated based on long-term data from the quarries. Loss on ignition (LOI) was determined by weighing before and after heating to 1000 °C in a laboratory muffle furnace. In addition, the elemental composition of the washing residue was characterized to assess whether it was likely that the surface materials originated in the quarries. The assessment was based mainly on the Ca concentration of the washing residue.

A predictive multi-component chemical equilibrium model was built based on commercially available databases and software and published thermodynamic data. The equilibrium model is based on the minimization of Gibbs free energy to determine the stable phases of the system. The equilibrium condition implies that kinetics is not considered; further, the model assumes that all elements have access to each other. Despite the limitations mentioned above, it has been proven to be a useful tool to predict and interpret phase systems of high temperatures. The model was used to obtain global phase diagrams of the high-order system in question, calculated as a function of temperature in the range 1000–1500 °C, corresponding to the high-temperature zone of the lime kiln. From the global phase diagrams, phase diagrams for Ca compounds were extracted. The diagrams for Ca compounds were utilized to analyze the impact of the impurities on limestone surfaces on the quicklime product quality. The model input was the elemental composition of samples, in both as-received and washed conditions, and comprised 15 elements: Al, C, Ca, Cl, Fe, H, K, Mg, Mn, Na, O, P, S, Si, and Ti. All calculations were made at 1 bar and in an atmosphere of 50 mol-% CO₂ and 50 mol-% O₂. Thermodynamic data from Lindberg et al. and Bale et al. [52,53] were used. The FactSage 7.3 software and FACTPS and FToxid databases, comprising pure solids, an oxide melt, and solid solutions for wollastonite (CaSiO₃ (ss)), bredigite (Ca₇Mg(SiO₄)₄ (ss)), olivine (Ca₂SiO₄ (ss)), melilite (Ca₂(Mg,Fe,Al)(Al,Fe,Si)₂O₇), calcium ferrite (Ca₂(Fe,Al)₂O₅ (ss) notation: C2AF (ss)), belite (Ca₂SiO₄ (ss) notation: C2S (ss)), calcium aluminate (Ca₃(Al,Fe)₂O₆ notation: C3A (ss)), and feldspar, were used. For the salt mixture system of Na-K-Ca-Cl-S-C-O, the database from Lindberg et al. was utilized.

3. Results

The elemental compositions, expressed as oxides, of the samples derived from limestone A and B, as determined by XRF, IR-C/S analysis, and LOI at 1000 °C, are presented in Table 3.

Table 3. Analysis results obtained for Limestone A and B, in wt.%, as determined by XRF and IR-C/S analysis, and loss on ignition at 1000 °C. Expressed as oxides. * Cl content was estimated based on long-term quarry data.

Limestone	A	A	A	B	B	B
Condition	As-Received	Washed	Washing Residue	As-Received	Washed	Washing Residue
CaO	54.06	54.14	47.39	54.06	54.43	44.31
MgO	0.47	0.46	1.02	0.76	0.71	2.65
SiO ₂	1.18	1.02	7.08	0.89	0.79	8.38
Al ₂ O ₃	0.39	0.33	2.32	0.32	0.27	2.63
Fe ₂ O ₃	0.17	0.14	0.88	0.19	0.18	2.12
MnO	0.10	0.10	0.12	0.02	0.02	0.04
P ₂ O ₅	0.02	0.02	0.06	0.01	0.01	0.03
Na ₂ O	0.05	0.05	0.46	0.06	0.05	0.24
TiO ₂	0.02	0.02	0.12	0.02	0.02	0.14
K ₂ O	0.12	0.10	0.71	0.09	0.07	0.87
S	0.04	0.03	0.24	0.05	0.05	0.17
Cl *	0.01	0.01	0.01	0.01	0.01	0.01
LOI	43.11	43.33	38.97	43.23	43.06	37.86
Sum	99.8	99.8	99.3	99.7	99.7	99.5

The elemental compositions for as-received and washed materials were used as input to the predictive multi-component chemical equilibrium model to determine the global phase diagrams of the resulting quicklime. From the global phase diagrams, phase diagrams for Ca compounds were extracted in the quicklime production temperature range of 1000–1500 °C. The resulting phase diagrams for Ca compounds are shown in Figures 1–4.

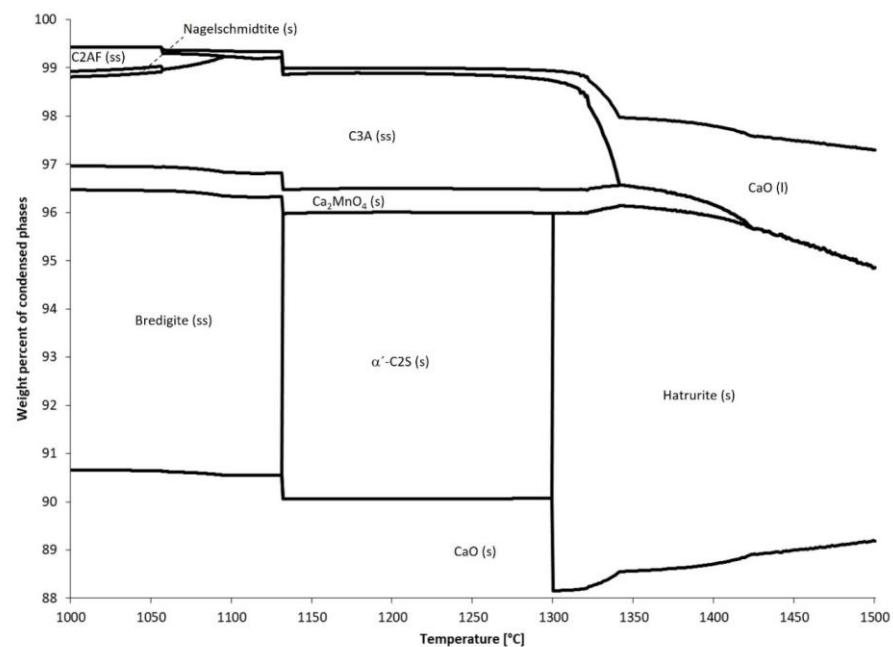


Figure 1. Phase diagram for calcium compounds in quicklime product of Limestone A in as-received condition. Extracted from the global phase diagram calculated from the elemental composition of the sample. CaO (l) was present in the oxide melt, and temperature (1000–1500 °C) was plotted against the weight percent of condensed phases.

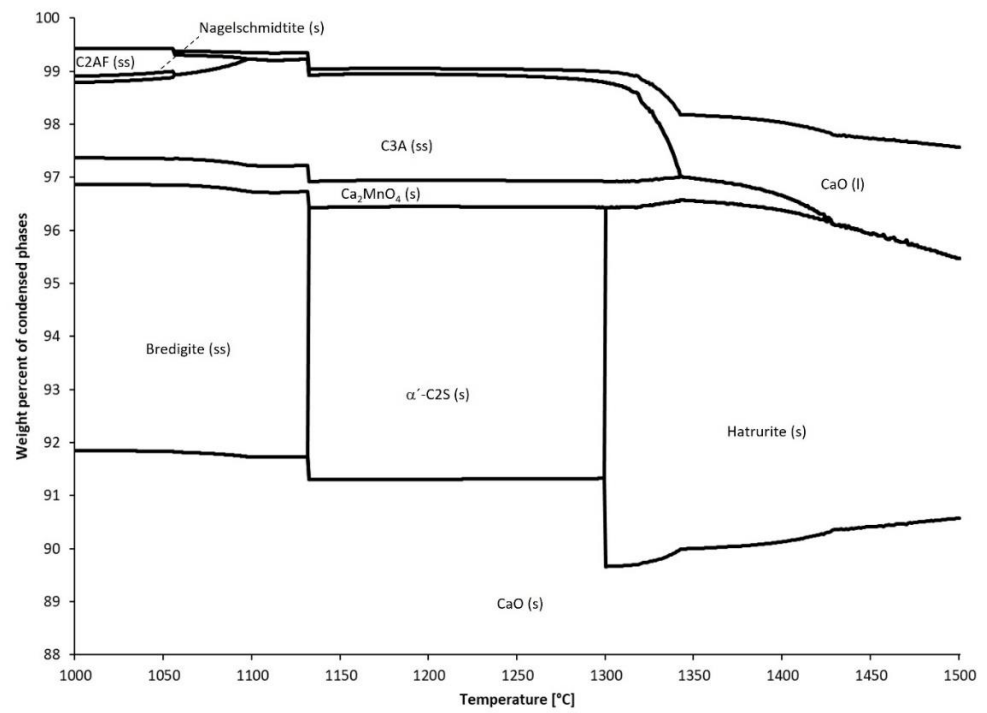


Figure 2. Phase diagram for calcium compounds in quicklime product of Limestone A in washed condition. Extracted from the global phase diagram calculated from the elemental composition of the sample. CaO (l) was present in the oxide melt, and temperature (1000–1500 °C) was plotted against the weight percent of condensed phases.

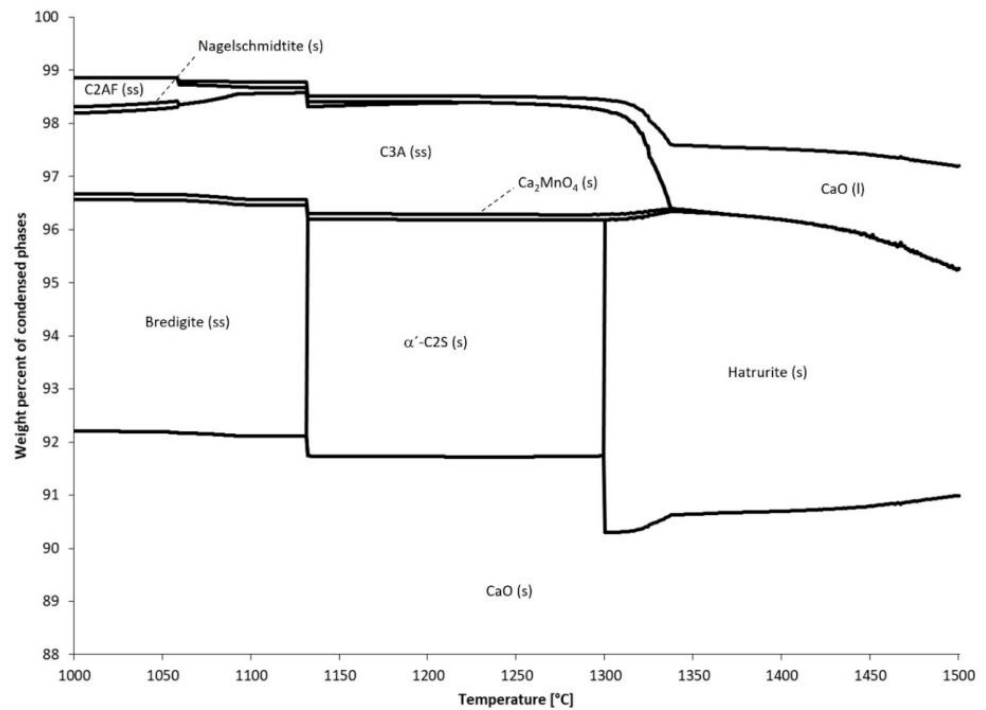


Figure 3. Phase diagram for calcium compounds in quicklime product of Limestone B in as-received condition. Extracted from the global phase diagram calculated from the elemental composition of the sample. CaO (l) was present in the oxide melt, and temperature (1000–1500 °C) was plotted against the weight percent of condensed phases.

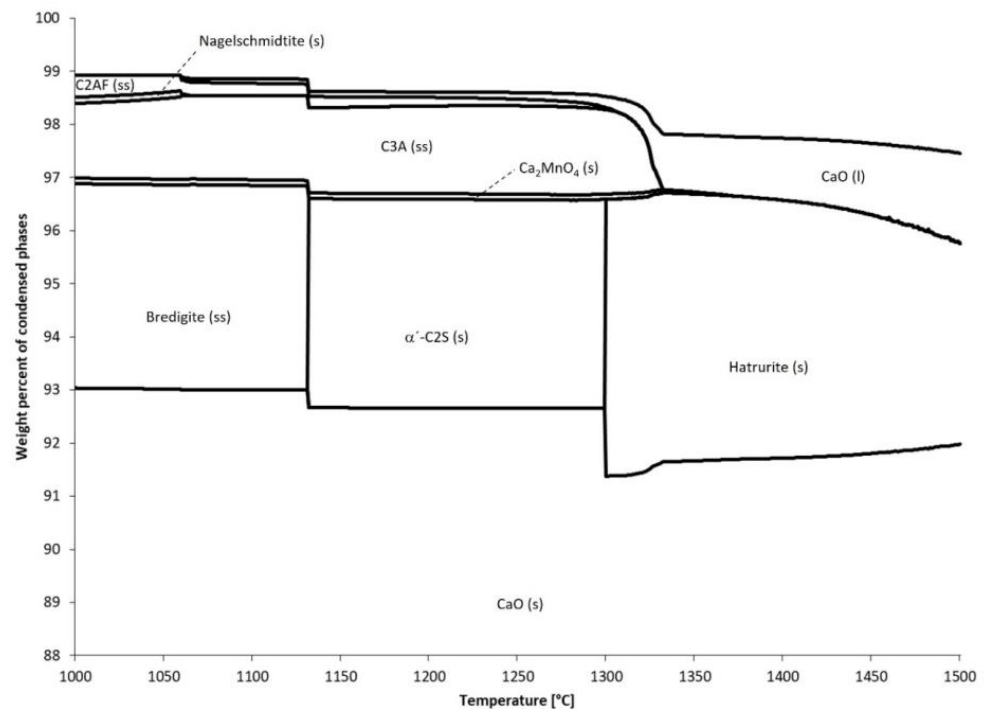


Figure 4. Phase diagram for calcium compounds in quicklime product of Limestone B in washed condition. Extracted from the global phase diagram calculated from the elemental composition of the sample. CaO (l) was present in the oxide melt, and temperature (1000–1500 °C) was plotted against the weight percent of condensed phases.

Figures 1–4 describe the phase evolution of Ca compounds expressed as the weight percent of condensed phases. The figures show the following:

That the phase evolution of Ca at 1000–1131 °C can be described as the formation of the following:

- 90.7–93.0 wt.% of CaO (s).
- 3.8–5.6 wt.% of Bredigite (ss), a solid solution originating from $\text{Ca}_7\text{Mg}(\text{SiO}_4)_4$ by the substitution of some Ca by Mg.
- 1.7–2.4 wt.% of calcium aluminate $\text{Ca}_3\text{Al}_2\text{O}_6$, designated C3A (ss), in solid solution with Fe and Na.
- 0.4–0.5 wt.% of calcium ferrite, designated C2AF (ss), a solid solution of $\text{Ca}_2\text{Fe}_2\text{O}_5$ with $\text{Ca}_2\text{Al}_2\text{O}_5$.
- 0.1–0.5 wt.% of Ca_2MnO_4 (s).
- Traces of Nagelschmidite (s), $\text{Ca}_7\text{P}_2\text{Si}_2\text{O}_{16}$.
- Traces of CaO (l), Ca dissolved into the oxide melt.

That in the temperature range 1132–1298 °C, the phase composition changed significantly when α' -C2S formed. The composition can be described as follows:

- 90.1–92.7 wt.% of CaO (s).
- 3.9–5.9 wt.% of alpha' belite, Ca_2SiO_4 , designated α' -C2S (s).
- 1.7–2.4 wt.% of C3A (ss).
- 0.1–0.5 wt.% of Ca_2MnO_4 (s).
- 0.2 wt.% of CaO (l), Ca dissolved into the oxide melt.

That at 1298–1500 °C, Hatrurite is formed, significantly influencing the phase composition. The composition in the temperature range 1298–1500 °C can be described as follows:

- 90.4–92.9 wt.% of CaO (s).
- 5.2–7.8 wt.% of Hatrurite (s), Ca_3SiO_5 (s).
- 1.6–2.3 wt.% of C3A (ss).

- 0.1–0.5 wt.% of Ca_2MnO_4 (s).
- 3.6–5.4 wt.% of CaO (l), Ca dissolved into the oxide melt.

4. Discussion

Quicklime has many quality parameters, such as reactivity [54], available lime, and residual CO_2 content [55]; however, in the present study, the chemical quality of quicklime is discussed in terms of the amount of calcium oxide, CaO (s), in the product, as described by the phase diagram for Ca phases.

The elemental compositions of the limestone samples, shown in Table 3, facilitated their chemical classification according to Table 1. Limestone A is of medium purity, with CaO content of 54.06 wt.% in the as-received condition and 54.14 wt.% after washing. The analyzed surface particles in the washing residue consisted mainly of Ca but showed high concentrations of impurities, mainly of Mg, Si, Al, and Fe. The surface impurities decreased the CaO content in the bulk feed by 0.08 wt.%. Limestone B is a medium- to high-purity limestone: the CaO content was 54.06 wt.% as-received and 54.43 wt.% after washing. The washing residue consisted mainly of Ca. The main impurities found in the washing residue were Si, Mg, Al, and Fe. Removing the surface impurities through washing increased the CaO content by 0.37 wt.%. For both A and B and the as-received and washed conditions, the impurities in the samples were consistent with typical levels for commercial limestone (see Table 2).

The surface particles, i.e., the washing residues, had a similar distribution of major elements to the washed rock, i.e., dominated by Ca and with a relatively high LOI, consistent with carbonate rock. It can thus be assumed that the surface particles originated from within the quarry areas and not from outside the quarry.

The predictive multi-component chemical equilibrium model was used to obtain phase diagrams of Ca compounds for the quicklime at kiln temperatures. The results are shown in Figures 1–4.

The predicted Ca phases are in accordance with earlier work. Vola detected, by X-ray diffraction, the main phases of calcium oxide (76–96 wt.%), Larnite (0–4 wt.%), Hatrurite (0–2 wt.%), Dicalcium manganate (2–6 wt.%), and Tricalcium aluminate (0–2 wt.%) in laboratory quicklime samples of different limestones cooled from 1050 °C and from 1150 °C [30]. In addition, some samples were reported to contain Gehlenite, Srebrodolskite, Merwinite and Anhydrite. Vola et al. also detected, by X-ray diffraction, the main calcium phases of calcium oxide (56–100 wt.%), Larnite (0–30 wt.%), Hatrurite (0–6 wt.%), Dicalcium manganate (0–3 wt.%), and Tricalcium aluminate (0–5 wt.%) in laboratory quicklime samples of different limestone cooled from 1200 °C [30]. In addition, some samples were reported to contain Gehlenite, Portlandite, and Brownmillerite.

Although the levels of impurities in the surface layers were high, clearly exceeding that of the washed rock, the Ca content of the as-received limestone samples was only marginally reduced (see Table 3). However, the results show that due to the interaction between Ca and the impurities, mainly Si, Al, and Fe as described by Reactions (2)–(6), and Mg and Mn by an unknown reaction mechanism, the CaO (s) content of the quicklime was significantly reduced. To highlight this effect and promote comparison between the as-received and washed samples, Figures 5 and 6 show the quality parameter of interest, CaO (s), extracted from phase diagrams of Ca compounds, seen in Figures 1–4, as a function of temperature. For all samples, CaO (s) reached a maximum at a temperature range of 1000–1100 °C. The minimum CaO (s) content was obtained near to the temperature of Hatrurite formation, at 1300 °C. At temperatures exceeding 1300 °C, the phase diagrams, seen in Figures 1–4, suggest that the equilibrium gradually shifted toward less Hatrurite and increased amounts of Ca being dissolved into the melt and an increased level of CaO (s). The stability of Hatrurite will depend on the global equilibrium, and it is reported to be 1799 °C in the CaO– SiO_2 system used in the calculations [53].

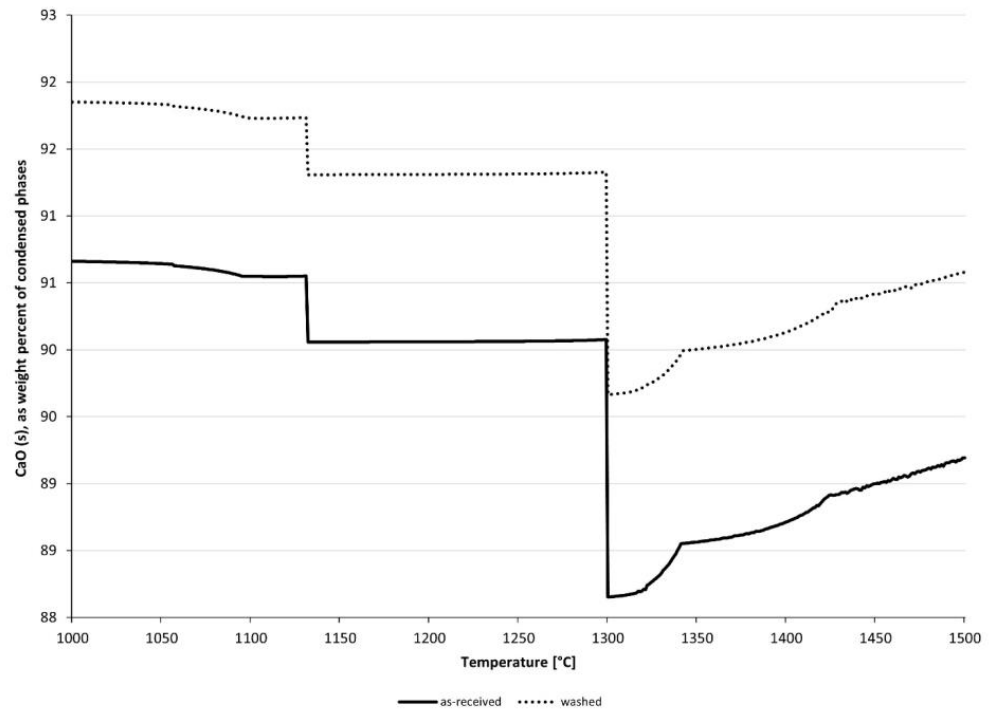


Figure 5. Limestone A, as-received and washed: CaO (s) in quicklime product, extracted from phase diagrams of Ca compounds seen in Figures 1 and 2, in weight percent of condensed phases.

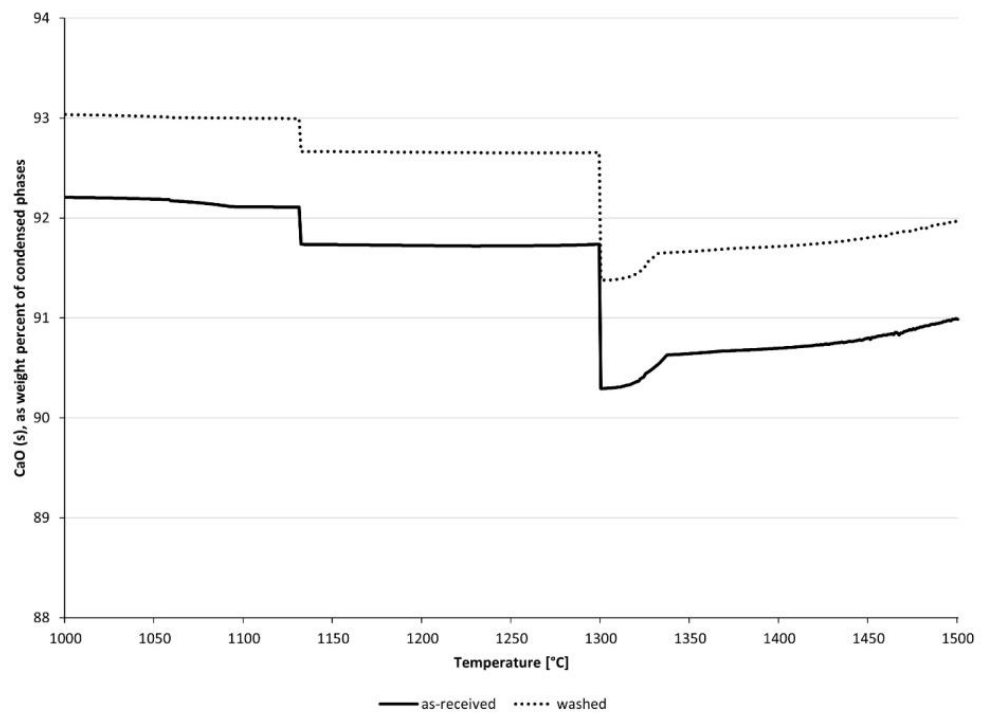


Figure 6. Limestone B, as-received and washed: predicted CaO(s) in quicklime product, extracted from phase diagrams of Ca compounds seen in Figures 3 and 4, in weight percent of condensed phases.

The results show that for Limestone A in an as-received condition, the CaO (s) content varied between 88.2 and 90.7 wt.%, and in a washed condition, it was between 89.7 and 91.9 wt.%, with the surface impurities reducing CaO (s) by 1.2–1.5 wt.%. For Limestone B in the as-received condition, CaO (s) varied between 90.3 and 92.2 wt.%, and in the washed

condition, it was between 91.4 and 93.0 wt.%, with the surface impurities reducing CaO (s) by 0.8–1.1 wt.%.

The results show that from a quicklime quality perspective, with respect to CaO (s), limestone should be processed below a maximum temperature of 1300 °C, which likely corresponds well to many current lime kiln design parameters. Above 1300 °C, the quality is reduced due to Hatrurite formation. The results also show that even if the surface impurities only marginally reduce the purity of the limestone, the impurities will reduce CaO (s) in the quicklime by the formation of Ca compounds other than CaO (s), mainly Bredigite, α' -C2S, C3A, and Hatrurite. For the investigated samples, the CaO (s) was reduced by 0.8–1.5 wt.%, which is significant from a quicklime product quality perspective. A limitation of the methods applied in this study is that all impurities were allowed to react with the bulk limestone and reach equilibrium conditions. In actual kiln operations, all reactions will not reach equilibrium, and since the quarry dust is located on the surface of the limestone pebbles, some of it is expected to be released, e.g., due to pebble–pebble abrasion in the kiln, and transported by the kiln gas flows.

The results could be assessed in relation to further investigations of the quarries, e.g., locating the main sources of quarry particulates with high concentrations of impurities, e.g., dust, mud, or clay, and undertaking actions to reduce limestone feed product exposure to impurities, e.g., by the encapsulation of equipment, or to remove adhered impurities, e.g., by washing. This could be combined with a follow-up analysis of the quantities and compositions of surface particulates for the purpose of verification.

5. Conclusions

Limestone quarry dust generally consists of fine particulates of limestone, mud, and clay, high in impurities. If adhered to limestone lump surfaces, the bulk concentration of impurities in limestone product is increased. The impacts of impurities adhered to the surface of two different limestone samples were investigated. The elemental compositions of the samples were determined through XRF and IR-C/S analysis. A predictive global multi-component chemical equilibrium model was designed based on the elemental composition of the samples. The temperature range of 1000–1500 °C was used, corresponding to the high-temperature zone of the lime kiln. From the global phase diagrams, phase diagrams for Ca compounds were extracted. The Ca compound phase diagrams show that the combined effects of impurities and kiln temperature on the main quicklime quality parameter, CaO (s), are significant. Since the price of a quicklime product is mainly dependent on the CaO (s) content, a washing protocol has the potential to increase the value of the product. The results create an opening for process optimization in the form of, e.g., limestone washing procedures and temperature control in kilns based on limestone compositional data. Based on the results, the following can be concluded:

- For both limestone samples, there was an accumulation of impurities on the surface. This material could be separated through washing. The washed rock samples had fewer impurities than the as-received samples and the washing residue. The composition of the washing residue indicated that the fine adhered materials likely originated from within the quarry.
- Surface particles affected the quality of quicklime products; the developed predictive multi-component chemical equilibrium model suggested a significant reduction in the main quality parameter of the quicklime, CaO (s), of 0.8–1.5 wt.% for the investigated materials, due mainly to the formation of Bredigite, α' -C2S, C3A, and Hatrurite.
- The amount of CaO (s) varied greatly with temperature. More impurities resulted in more variation and a greater need for accurate temperature control of the kiln, where keeping the temperature below approximately 1300 °C, that of Hatrurite formation, allows for a product with higher CaO (s) content.

Author Contributions: Conceptualization, M.E., K.S., M.C. and M.B.; Methodology, M.E., K.S., M.C. and M.B.; Formal Analysis, M.E.; Investigation, M.E.; Writing—Original Draft Preparation, M.E.;

Writing—Review and Editing, M.E., K.S., M.C. and M.B.; Visualization, M.E. and K.S.; Supervision, M.E. and M.B.; Project Administration, M.E. and M.B.; Funding Acquisition, M.E. and M.B. All authors have read and agreed to the published version of the manuscript.

Funding: This research was funded by Swedish Energy Agency grant number 50224-1, Industrial Doctoral School for Research and Innovation grant number 2019; The Ellen, Walter and Lennart Hesselman Foundation grant number 2022, and VINNOVA grant number 2015-04541.

Data Availability Statement: The raw data supporting the conclusions of this article will be made available by the authors on request.

Acknowledgments: Krister Backlund is acknowledged for the geological description of the limestone samples. Nordkalk AB, SMA Mineral AB, Heidelberg Materials Cement Sverige AB, the Ellen, Walter and Lennart Hesselman Foundation, the Swedish Mineral Processing Research Association—MinFo, the Industrial Doctoral School for Research and Innovation at Umeå University, Vinnova, and the Swedish Energy Agency are acknowledged for project support.

Conflicts of Interest: The authors declare no conflicts of interest.

References

1. García-Labiano, F.; Abad, A.; De Diego, L.F.; Gayán, P.; Adánez, J. Calcination of calcium-based sorbents at pressure in a broad range of CO₂ concentrations. *Chem. Eng. Sci.* **2002**, *57*, 2381–2393. [[CrossRef](#)]
2. Bai, R.; Li, N.; Liu, Q.; Chen, S.; Liu, Q.; Zhou, X. Effect of Steam on Carbonation of CaO in Ca-Looping. *Molecules* **2023**, *28*, 4910. [[CrossRef](#)]
3. Fiquet, G.; Guyot, F.; Itie, J.-P. High-pressure X-ray diffraction study of carbonates: MgCO₃, CaMg(CO₃)₂, and CaCO₃. *Am. Miner.* **1994**, *79*, 15–23.
4. Galan, I.; Glasser, F.P.; Andrade, C. Calcium carbonate decomposition. *J. Therm. Anal. Calorim.* **2013**, *111*, 1197–1202. [[CrossRef](#)]
5. Smadi, E.; Chinnici, A.; Dally, B.; Nathan, G.J. Effect of heating rate on the kinetics of limestone calcination. *Chem. Eng. J.* **2023**, *475*, 146165. [[CrossRef](#)]
6. Huang, J.-M.; Daugherty, K.E. Catalytic effect of alkali carbonates on the calcination of calcium carbonate. *Thermochim. Acta* **1987**, *115*, 57–62. [[CrossRef](#)]
7. Calvo, E.G.; Arranz, M.A.; Letón, P. Effects of impurities in the kinetics of calcite decomposition. *Thermochim. Acta* **1990**, *170*, 7–11. [[CrossRef](#)]
8. Gupta, P.; De, A.; Biswas, C. The effect of impurities on the calcination behaviour of CaCO₃ nuggets. *J. Eng. Res.* **2017**, *5*, 34–45.
9. Hyatt, E.P.; Cutler, I.B.; Wadsworth, M.E. Calcium Carbonate Decomposition in Carbon Dioxide Atmosphere. *J. Am. Ceram. Soc.* **1958**, *41*, 70–74. [[CrossRef](#)]
10. Valverde, J.M.; Medina, S. Crystallographic transformation of limestone during calcination under CO₂. *Phys. Chem. Chem. Phys.* **2015**, *17*, 21912–21926. [[CrossRef](#)]
11. Yang, J.; Fu, L.-Y.; Zhang, W.; Wang, Z. Mechanical property and thermal damage factor of limestone at high temperature. *Int. J. Rock Mech. Min. Sci.* **2019**, *117*, 11–19. [[CrossRef](#)]
12. Valverde, J.M.; Sanchez-Jimenez, P.E.; Perez-Maqueda, L.A. Limestone Calcination Nearby Equilibrium: Kinetics, CaO Crystal Structure, Sintering and Reactivity. *J. Phys. Chem. C* **2015**, *119*, 1623–1641. [[CrossRef](#)]
13. Ontiveros-Ortega, E.; Ruiz-Agudo, E.M.; Ontiveros-Ortega, A. Thermal decomposition of the CaO in traditional lime kilns. Applications in cultural heritage conservation. *Constr. Build. Mater.* **2018**, *190*, 349–362. [[CrossRef](#)]
14. Maya, J.C.; Chejne, F.; Gómez, C.A.; Bhatia, S.K. Effect of the CaO sintering on the calcination rate of CaCO₃ under atmospheres containing CO₂. *AIChE J.* **2018**, *64*, 3638–3648. [[CrossRef](#)]
15. Eriksson, M.; Carlborg, M.; Broström, M. Characterization of ring deposits inside a quicklime producing long rotary kiln. *Energy Fuels* **2019**, *33*, 11731–11740. [[CrossRef](#)]
16. Piringier, H. Lime Shaft Kilns. *Energy Procedia* **2017**, *120*, 75–95. [[CrossRef](#)]
17. Vola, G.; Ardit, M.; Frijia, G.; Di Benedetto, F.; Fornasier, F.; Lugli, F.; Natali, C.; Sarandrea, L.; Schmitt, K.E.; Cipriani, A. Characterization and Provenance of Carbonate Rocks for Quicklime and Dolomite Production in Twin-Shaft Regenerative Kilns from the Arabian Peninsula and Neighboring Countries. *Minerals* **2023**, *13*, 1500. [[CrossRef](#)]
18. Vola, G.; Sarandrea, L.; Mazziere, M.; Bresciani, P.; Ardit, M. Reactivity and overburning tendency of quicklime burnt at high temperature. *ZKG Int.* **2019**, *72*, 20–31.
19. Vola, G.; Sarandrea, L.; Della Porta, G.; Cavallo, A.; Jadoul, F.; Cruciani, G. The influence of petrography, mineralogy and chemistry on burnability and reactivity of quicklime produced in Twin Shaft Regenerative (TSR) kilns from Neoproterozoic limestone (Transvaal Supergroup, South Africa). *Mineral. Petrol.* **2018**, *112*, 555–576. [[CrossRef](#)]
20. Moropoulou, A.; Bakolas, A.; Aggelakopoulou, E. The effects of limestone characteristics and calcination temperature to the reactivity of the quicklime. *Cem. Concr. Res.* **2001**, *31*, 633–639. [[CrossRef](#)]
21. Piringier, H. The Maerz hybrid kiln for variable lime reactivity. *ZKG Int.* **2020**, *73*, 56–60.

22. Cwik, K.; Broström, M.; Backlund, K.; Fjäder, K.; Hiljanen, E.; Eriksson, M. Thermal Decrepitation and Thermally-Induced Cracking of Limestone Used in Quicklime Production. *Minerals* **2022**, *12*, 1197. [[CrossRef](#)]
23. Sandström, K.; Eriksson, M.; Broström, M. Solid biofuel combustion or electrification for limestone calcination: Effects on quicklime surface microstructure. *Fuel* **2022**, *326*, 124955. [[CrossRef](#)]
24. Sandström, K.; Broström, M.; Eriksson, M. Coal ash and limestone interactions in quicklime production. *Fuel* **2021**, *300*, 120989. [[CrossRef](#)]
25. Schlegel, T.; Padox, G. Modelled fate of sulphur and chlorine rotary lime kilns Part I. *ZKG Int.* **2018**, *71*, 66–75.
26. Silva, M.; Specht, E.; Schmidt, J. Thermophysical properties of limestone as a function of origin (PART 1): Specific heat capacities. *ZKG Int.* **2010**, *63*, 55–62.
27. Sandaka, G.; Al-Karawi, J.; Specht, E.; Silva, M. Thermophysical properties of lime as a function of origin (Part 4): Thermal conductivity. *ZKG Int.* **2017**, *70*, 36–41.
28. Vola, G.; Ardit, M.; Sarandrea, L.; Brignoli, G.; Natali, C.; Cavallo, A.; Bianchini, G.; Cruciani, G. Investigation and prediction of sticking tendency, blocks formation and occasional melting of lime at HT (1300 °C) by the overburning test method. *Constr. Build. Mater.* **2021**, *294*, 123577. [[CrossRef](#)]
29. Vola, G. High-Grade Burnt Lime Products: Impact of Calcination Kinetics on Slaking Reactivity, Sticking Tendency and Blocks Formation at HT (1300 °C). Ph.D. Thesis, Università degli Studi di Ferrara, Ferrara, Italy, 2019. Available online: <https://hdl.handle.net/11392/2488317> (accessed on 7 July 2018).
30. Vola, G.; Bresciani, P.; Rodeghero, E.; Sarandrea, L.; Cruciani, G. Impact of rock fabric, thermal behavior, and carbonate decomposition kinetics on quicklime industrial production and slaking reactivity. *J. Therm. Anal. Calorim.* **2019**, *136*, 967–993. [[CrossRef](#)]
31. Eriksson, M.; Hökfors, B.; Backman, R. Oxyfuel combustion in rotary kiln lime production. *Energy Sci. Eng.* **2014**, *2*, 204–215. [[CrossRef](#)]
32. Hökfors, B.; Eriksson, M.; Backman, R. Improved Process Modeling for a Lime Rotary Kiln Using Equilibrium Chemistry. *J. Eng. Technol.* **2012**, *29*, 8–18.
33. Eriksson, M.; Hökfors, B.; Backman, R. The Effects of Oxygen Enrichment and Fuel Composition on Rotary Kiln Lime Production. *J. Eng. Technol.* **2015**, *32*, 30–43.
34. Taylor, H.F.W. *Cement chemistry*; Thomas Telford Publishing: London, UK, 1997; p. 459.
35. Hills, L.M.; Johansen, V.; Miller, F.M. Solving raw material challenges In Proceedings of the IEEE-IAS/PCS 2002 Cement Industry Technical Conference. Conference Record (Cat. No. 02CH37282), Jacksonville, FL, USA, 5–9 May 2002.
36. Viggh, E.; Eriksson, M.; Wilhelmsson, B.; Backman, R. Early formation of belite in cement clinker raw materials with slag. *Adv. Cem. Res.* **2021**, *33*, 249–256. [[CrossRef](#)]
37. Telschow, S.; Frandsen, F.; Theisen, K.; Dam-Johansen, K. Cement Formation—A Success Story in a Black Box: High Temperature Phase Formation of Portland Cement Clinker. *Ind. Eng. Chem. Res.* **2012**, *51*, 10983–11004. [[CrossRef](#)]
38. Manocha, S.; Ponchon, F. Management of Lime in Steel. *Metals* **2018**, *8*, 686. [[CrossRef](#)]
39. Apodaca, L.E. Lime. In *2018 Minerals Yearbook*; U.S. Department of the Interior U.S. Geological Survey: Reston, VA, USA, 2021.
40. Dowling, A.; O'Dwyer, J.; Adley, C.C. Lime in the limelight. *J. Clean. Prod.* **2015**, *92*, 13–22. [[CrossRef](#)]
41. Eriksson, M. Sustainability Measures in Quicklime and Cement Clinker Production. Doctoral Thesis, Department of Applied Physics and Electronics, Umeå University, Umeå, Sweden, 2015. Available online: <http://urn.kb.se/resolve?urn=urn:nbn:se:umu:diva-112842> (accessed on 7 July 2018).
42. Schorcht, F.; Kourti, I.; Scalet, B.M.; Roudier, S.; Sancho, L.D. Best Available Techniques (BAT) Reference Document for the Production of Cement, Lime and Magnesium Oxide. Joint Research Centre of the European Commission, Institute for Prospective Technological Studies: Luxemburg, 2013. Available online: <https://ec.europa.eu/jrc/en/publication/reference-reports/best-available-techniques-bat-reference-document-production-cement-lime-and-magnesium-oxide> (accessed on 27 March 2014).
43. Survey, U.S.G. *Mineral commodity summaries 2023*; U.S. Geological Survey: Reston, VA, USA, 2023; p. 201.
44. Boynton, R.S. *Chemistry and Technology of Lime and Limestone*; John Wiley & Sons, Inc.: New York, NY, USA, 1966.
45. Van Ranst, E.; Mees, F.; Bock, L.; Langohr, R. Development of a clay-rich interval above a limestone substrate in the Condroz region of southern Belgium. *CATENA* **2014**, *121*, 204–213. [[CrossRef](#)]
46. Searle, A.B. *Limestone and Its Products: Their-Nature, Production, and Uses*; Ernest Benn Limited: London, UK, 1935; p. 709.
47. Harrison, D.J.; Adlam, K.A. *The Limestone and Dolomite Resources of the Peak District of Derbyshire and Staffordshire*; British Geological Survey: Keyworth, Nottingham, 1984; p. 52.
48. Cox, F.C.; Bridge, M.; Hull, J.H. *Procedure for the Assesment of Limestone Resources*; Institute of Geological Sciences: Keyworth, Nottingham, 1977; p. 16.
49. Mitchell, C. High purity limestone quest. *Ind. Miner.* **2011**, *531*, 48–51.
50. Mitchell, C. High-purity limestone assessment: From mine to market. In *Lecture at Investment Opportunities in Saudi Industrial Minerals Workshop, Jeddah, Saudi Arabia, 9 March 2009*; British Geological Survey: Keyworth, Nottingham, 2009; pp. 1–20.
51. Backman, R.; Hupa, M.; Tran, H.N. Modelling the Sodium Enrichment in Lime Kilns. In Proceedings of the 1992 International Chemical Recovery Conference, Seattle, WA, USA, 7–11 June 1992; pp. 153–160.

52. Lindberg, D.; Backman, R.; Chartrand, P.; Hupa, M. Towards a comprehensive thermodynamic database for ash-forming elements in biomass and waste combustion—Current situation and future developments. *Fuel Process. Technol.* **2013**, *105*, 129–141. [[CrossRef](#)]
53. Bale, C.W.; Bélisle, E.; Chartrand, P.; Decterov, S.A.; Eriksson, G.; Gheribi, A.E.; Hack, K.; Jung, I.H.; Kang, Y.B.; Melançon, J.; et al. FactSage thermochemical software and databases, 2010–2016. *Calphad* **2016**, *54*, 35–53. [[CrossRef](#)]
54. *EN 459-2:2010*; Building Lime-Part 2: Test Methods. SIS Förlag; CEN: Stockholm, Sweden, 2010.
55. *ASTM C25-19*; Standard Test Methods for Chemical Analysis of Limestone, Quicklime, and Hydrated Lime C 25-06. ASTM: West Conshohocken, PA, USA, 2006; p. 36.

Disclaimer/Publisher’s Note: The statements, opinions and data contained in all publications are solely those of the individual author(s) and contributor(s) and not of MDPI and/or the editor(s). MDPI and/or the editor(s) disclaim responsibility for any injury to people or property resulting from any ideas, methods, instructions or products referred to in the content.